ChemComm

COMMUNICATION

View Article Online
View Journal | View Issue

Cite this: *Chem. Commun.*, 2022, **58**, 4223

Received 14th January 2022,
Accepted 18th February 2022

DOI: 10.1039/d2cc00258b

rsc.li/chemcomm

Twofold rattling mode-induced ultralow thermal conductivity in vacancy-ordered double perovskite Cs_2SnI_6†

Un-Gi Jong, *[a] Yun-Sim Kim,[a] Chol-Hyok Ri,[a] Yun-Hyok Kye,[a] Chol-Jin Pak,[a] Stefaan Cottenier [b] and Chol-Jun Yu *[a]

We report a first-principles study of lattice vibrations and thermal transport in Cs_2SnI_6, the vacancy-ordered double perovskite. Twofold rattlers of Cs atoms and SnI6 clusters in Cs_2SnI_6, being different from $CsSnI_3$ with only Cs atom rattlers, largely scatter heat-carrying acoustic phonons strongly coupled with low-lying optical phonons and lower phonon group velocity. Using renormalized phonon dispersions at finite temperatures, we reveal that anharmonicity and twofold rattling modes induce an ultralow thermal conductivity at room temperature.

Novel thermoelectrics with ultralow thermal conductivity are key ingredients in driving future energy technologies such as thermoelectric energy conversion.[1] The lattice thermal conductivity in a crystalline solid is $\kappa = \sum_{q\lambda} C_{q\lambda}|v_{q\lambda}|^2\tau_{q\lambda}$ with the heat capacity C, phonon group velocity v and phonon lifetime τ, which are dependent on the momentum q and mode λ of the phonon.[2,3] The key to decreasing the thermal conductivity is to reduce the phonon lifetimes through increasing the phonon–phonon scattering, *i.e.*, anharmonic phonon interactions, as revealed in disorder-free systems like SnSe[4–6] and PbTe.[7,8] Strong phonon–phonon scattering is especially manifested *via* the localized vibration motion of constituent atoms in optical modes, coupled with and scattering heat-carrying acoustic phonons, so-called rattling modes.[9–14] This mechanism is broadly applied to explain the low thermal conductivity in cage-like crystal structures like skutterudites and clathrates with atomic rattlers[10,12,14] and layered structures with Cu atom dimer rattlers.[9]

The halide perovskites (HPs) span hybrid organic–inorganic and all-inorganic materials with a chemical formula ABX_3 (A = CH_3NH_3, Cs; B = Pb, Sn, Ge; X = I, Br, Cl) and are extremely anharmonic materials.[15–18] In these materials, the atomistic dynamics of A-site cations is highly complex and anharmonic, *i.e.*, rotational motion for the organic molecule[19–21] and cluster rattling motion for the inorganic atoms,[11,22] while BX_6 octahedra display distortions and tilting modes. These complex atomistic motions and anharmonic phonons result in a synergy that can originate their ultralow thermal conductivity.

The so-called double HPs, typically $Cs_2AgBiBr_6$[23–25] formed by replacing the two divalent Pb^{2+} cations with a pair of monovalent Ag^+ and trivalent Bi^{3+} cations, are envisioned to resolve severe issues of poor long-term stability and toxicity of lead in the single lead HPs. Moreover, theoretical investigation[25] found that $Cs_2AgBiBr_6$ in the cubic phase presents highly anharmonic phonons, leading to the ultralow thermal conductivity of 0.33 W m^{-1} K^{-1} at room temperature. Likewise, the vacancy-ordered double HPs, where half of the divalent cations are removed, exhibit the strong anharmonicity of lattice dynamics,[26–29] expecting a reduction of lattice thermal conductivity. Nevertheless, the underlying nature of the anharmonic phonon–phonon interactions and its consequences in the vacancy-ordered double HPs remain unknown.

In the present work, we thoroughly investigate the nature of lattice dynamics and temperature-dependent thermal conductivity of vacancy-ordered double perovskite $Cs_2Sn\bigcirc I_6$ in a simple cubic phase, where ○ is a vacancy, employing first-principles lattice dynamics calculations connected with explicit many-body theory calculations. For convenience, we denote $Cs_2Sn\bigcirc I_6$ as Cs_2SnI_6 hereafter. We provide a systematic comparison with its single counterpart $CsSnI_3$, demonstrating that twofold rattling motions of both Cs atoms and SnI_6 clusters induce ultralow thermal conductivity of 0.11 W m^{-1} K^{-1} even at room temperature in Cs_2SnI_6, which is almost one sixth of that in $CsSnI_3$ with only Cs rattling.

We start with scrutiny of the crystalline structure of cubic Cs_2SnI_6 with space group $Fm\bar{3}m$, comparing to cubic $CsSnI_3$

[a] *Chair of Computational Materials Design (CMD), Faculty of Materials Science, Kim Il Sung University, Pyongyang, PO Box 76, Democratic People's Republic of Korea. E-mail: ug.jong@ryongnamsan.edu.kp, cj.yu@ryongnamsan.edu.kp*

[b] *Department of Electromechanical, Systems and Metal Engineering and Center for Molecular Modeling (CMM), Ghent University, Technologiepark-Zwijnaarde 46, BE-9052 Gent, Belgium*

† Electronic supplementary information (ESI) available: Details of computational methods, convergence test for harmonic phonons, κ_l of $CsSnI_3$ at different q-point meshes, anharmonic phonon dispersions, cumulative κ_l, and average τ_{3rd} and v_g at various temperatures for $CsSnI_3$ and Cs_2SnI_6. See DOI: 10.1039/d2cc00258b

with space group $Pm\bar{3}m$. As shown in Fig. S1(a and b) in the ESI,† the crystal structure of Cs_2SnI_6 can be regarded as a defect variant of $CsSnI_3$ with isolated SnI_6 octahedra bridged by Cs atoms, which is in striking contrast to the corner-sharing arrangement of octahedra in $CsSnI_3$.[27–29] In spite of such structural changes, the local coordination environments of Cs atoms do not alter distinctly, as they reside in the ideal 12-coordinated cub-octahedral geometry formed by I atoms (Fig. S1(b), ESI†). Only the Cs–I bond length is slightly contracted from 4.37 Å in $CsSnI_3$ to 4.13 Å in Cs_2SnI_6. This is correlated with decreases of Sn–I bond length and lattice constant caused by the ordered Sn vacancies in Cs_2SnI_6. Note that the Cs–I distance of 4.13 Å in Cs_2SnI_6 is still longer than that of 3.92 Å in the cubic CsI crystalline solid and the sum of ionic radii of Cs^+ and I^- (3.87 Å). Therefore, it is clear that in Cs_2SnI_6, Cs atoms are located inside the over-sized cub-octahedral cage, expecting their role as a heavy rattler, which can drive the lattice anharmonicity as in $CsSnI_3$.

Meanwhile, the local environment of SnI_6 octahedra is significantly changed. In Cs_2SnI_6, they are isolated and located inside the over-sized cage-like structures composed of the Cs atoms. This is in contrast to the corner-sharing arrangement of SnI_6 octahedra in $CsSnI_3$ (Fig. S1(a), ESI†). Owing to the sufficient interstitial space in the cage-like structures, the isolated octahedra in Cs_2SnI_6 are loosely bound to their neighbors, so that they can play a similar role to the Cs atom rattlers. However, the corner-sharing octahedra in $CsSnI_3$ are tightly connected with each other, thereby implying impossibility for them to act as rattlers. Therefore, we can suppose both Cs atoms and isolated SnI_6 octahedra to be rattlers, indicating twofold rattling motions in Cs_2SnI_6. When compared to $CsSnI_3$ with only Cs atom rattlers, the lattice anharmonicity can be further enhanced in Cs_2SnI_6.

In order to verify this hypothesis of the twofold rattling mechanism, we performed lattice dynamics calculations for Cs_2SnI_6 and $CsSnI_3$ using supercells to obtain their phonon energies and density of states (DOS). Fig. 1(a and c) show the phonon dispersion curves and total DOS calculated at 0 K for $CsSnI_3$ and Cs_2SnI_6 (see Fig. S3 for the convergence test of phonon dispersions, ESI†). Note that the phonon dispersion curves obtained in this work are in good agreement with the previous calculations obtained by different methods.[27,30] For $CsSnI_3$, the soft phonon modes with the imaginary phonon energies are identified at M and R points of the Brillouin zone (BZ). This is in agreement with the recent experimental findings that $CsSnI_3$ can be stabilized in a cubic phase only at high temperatures over 441 K and transformed to tetragonal $P4/mbm$ at 362 K and to orthorhombic $Pnma$ phases at room temperature.[22] The soft phonon modes are also found at the Γ point for Cs_2SnI_6, which is at odds with the experimental observation that Cs_2SnI_6 can adopt the cubic structure at the whole range of temperatures.[31,32] As Xie *et al.*[22] already pointed out that the major reason for the anharmonic phonon modes in cubic $CsSnI_3$ is the Cs atom rattlers, moving away from the center of the cub-octahedral cage due to the local distortion of SnI_6 octahedra, the anharmonic phonon modes present even in the dynamically stable cubic Cs_2SnI_6 are associated with the rattlers. That is, they are just caused by the twofold rattling vibrations of the Cs atoms and octahedral clusters, as expected above.

The emergence of such imaginary phonon modes requires anharmonic phonon renormalization (APRN) at finite temperatures.[33,34] To this end, we performed self-consistent phonon (SCP) calculations to consider the anharmonic effects when elevating the temperature. In Fig. 1(a and c), we also show the calculated anharmonic phonon dispersion curves at finite

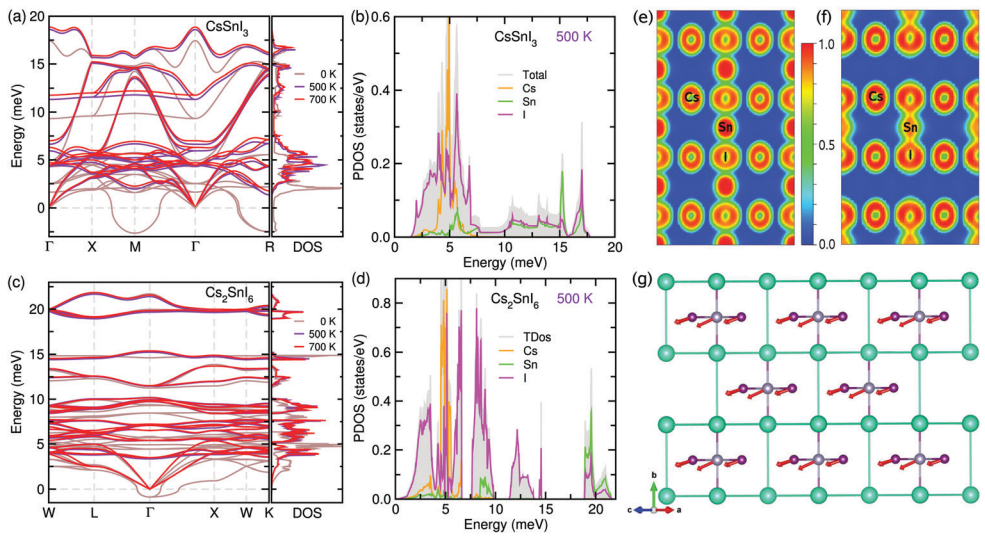

Fig. 1 Phonon dispersions and density of states (DOS) at 0, 500 and 700 K in (a) $CsSnI_3$ and (c) Cs_2SnI_6. Atom-projected phonon density of states (PDOS) at 500 K in (b) $CsSnI_3$ and (d) Cs_2SnI_6. Electron localization functions in the (110) planes of (e) $CsSnI_3$ and (f) Cs_2SnI_6. (g) Collective motion of Sn and I atoms in the host cages of Cs atoms, corresponding to phonon eigenvectors of the lowest optical mode (λ = 4) at the phonon energy of around 3.4 meV at the Γ point in Cs_2SnI_6, where green-, gray- and purple-colored balls represent Cs, Sn and I atoms, and red-colored arrows indicate the movement directions of atoms.

temperatures of 500 and 700 K for $CsSnI_3$ and Cs_2SnI_6 (see Fig. S4 and S5 for anharmonic phonon dispersions at different temperatures for Cs_2SnI_6 and $CsSnI_3$, ESI†). When compared with the harmonic phonon dispersions at 0 K, the imaginary phonon eigenvalues were found to become real by renormalization, demonstrating that the cubic phases for both $CsSnI_3$ and Cs_2SnI_6 become dynamically stable at high temperatures. Going from 0 K to finite temperatures, both the acoustic and optical modes for $CsSnI_3$ are distinctly changed in the whole range of phonon frequency, whereas the change was not radical for Cs_2SnI_6. This also indicates the thermal instability of cubic $CsSnI_3$ at 0 K, and relatively high stability of Cs_2SnI_6.

Importantly, the acoustic modes of Cs_2SnI_6 become flattened on going from the BZ center to the BZ boundary of around 5 meV of phonon energy in contrast with those of $CsSnI_3$ that are still quite dispersive, while all the optical modes of $CsSnI_3$ look more dispersive along arbitrary directions in the BZ compared with those of Cs_2SnI_6. Moreover, the lowest optical modes appear at about 3.4 meV in the acoustic region at the Γ point for Cs_2SnI_6 but not for $CsSnI_3$, revealing a strong coupling between low-lying optical and heat-carrying acoustic modes in Cs_2SnI_6 (see Fig. S11, ESI†). The strong optic-acoustic coupling is discernible from the distinctive avoided-crossing behaviour between the lowest optical and longitudinal acoustic branches in Cs_2SnI_6.[35] These low-lying optical modes coupled and avoided-crossing with the acoustic modes are recognized as strong rattling modes,[14,35] being responsible for a two order smaller phonon lifetime τ_{3rd} (see Fig. S12, ESI†) and a slower phonon group velocity v_g in Cs_2SnI_6 than in $CsSnI_3$. Therefore, we conceive that such optical modes act as strong scattering centers for heat-carrying acoustic phonons in Cs_2SnI_6.

To further understand the difference in lattice vibration between $CsSnI_3$ and Cs_2SnI_6, we plot their atom-projected phonon DOS (PDOS) calculated from the SCP calculations at 500 K in Fig. 1(b and d). Both HPs are found to have low-lying optical phonon modes around $\sim$5 meV, which are mostly associated with the rattling vibrations of Cs atoms. The Cs-related PDOS in Cs_2SnI_6 looks narrower than in $CsSnI_3$, verifying its stronger rattling vibrations of Cs atoms. Moreover, we observe separate peaks around 3.1, 5.0, 6.3 and 8.1 meV in the acoustic and low-lying optical regions for Cs_2SnI_6, which are mainly ascribed to the vibrations of I atoms with small contributions of Sn atoms. By contrast, a united peak is seen in the region between 3 and 7 meV for $CsSnI_3$. We can see a two orders of magnitude smaller τ_{3rd} within the phonon energies ranging from 0 to 10 meV (see Fig. S13, ESI†), and this distinct drop of the τ_{3rd} coincides with the additional separate peaks in the phonon DOS of Cs_2SnI_6. These additional peaks can be regarded as evidence for rattling vibrations of SnI_6 octahedral clusters, *i.e.*, collective motions of Sn and I atoms, as depicted in Fig. 1(g).

We analyze their electron localization functions (ELFs), as shown in Fig. 1(e and f), since these functions estimate the degree of electron localization in solids taking into account the local influence of the Pauli repulsion.[36] As the ELF value increases, the electrons are found to be more localized and thus the atomic bonds become stronger. Obviously, no charge is observed between the neighbouring octahedra due to the vacancies in Cs_2SnI_6 in contrast with $CsSnI_3$. This implies that the SnI_6 octahedral clusters in Cs_2SnI_6 are loosely bound to the neighbours, explaining the electronic origin of the cluster-rattling vibrations. In addition, non-spherical ELFs around Sn and I atoms in Cs_2SnI_6, reflecting the inhomogeneous connectivity of constituent atoms, explain the electronic origin of phonon anharmonicity.[37]

We finally calculated the lattice thermal conductivities of Cs_2SnI_6 and $CsSnI_3$ by solving the Boltzmann transport equation (BTE) within perturbation theory combined with the solution of the SCP equation. Fig. 2(a and b) show the phonon lifetimes τ_{3rd} and phonon group velocities v_g as functions of phonon energy, calculated from the SCP solution at 500 K considering the three-phonon scattering (see Fig. S6 and S7 for cumulative κ_l, and average τ_{3rd} and v_g, ESI†). When compared with $CsSnI_3$, τ_{3rd} in Cs_2SnI_6 is found to decrease more rapidly with decreasing phonon energy below 7.5 meV, which is ascribed to the aforementioned twofold rattling vibrations of Cs atoms and the octahedral clusters. To quantitatively assess the contribution of the atomic species, we estimated the mean square displacement (MSD) of atoms with increasing temperature, revealing that in $CsSnI_3$, Cs atoms have 1.8 and 5.1 times larger MSD than I and Sn atoms, whereas in Cs_2SnI_6, I atoms have 1.2 and 2.9 times larger MSD than Cs and Sn atoms (see Fig. S10, ESI†). Although the MSD of Cs atoms becomes smaller than that of I atoms in Cs_2SnI_6, the Cs (I) atoms in Cs_2SnI_6 still have slightly (much) larger MSD than those in $CsSnI_3$. These results verify the Cs atom rattling in $CsSnI_3$ and twofold rattling of Cs atoms and SnI_6 octahedra in Cs_2SnI_6. Moreover, v_g in Cs_2SnI_6 is observed to be smaller in the whole range of phonon energy. Cs_2SnI_6 has smaller heat capacity C_V than $CsSnI_3$ in the whole range of temperature because of the lack of Sn–I bonds due to the Sn vacancies (see Fig. S8, ESI†).

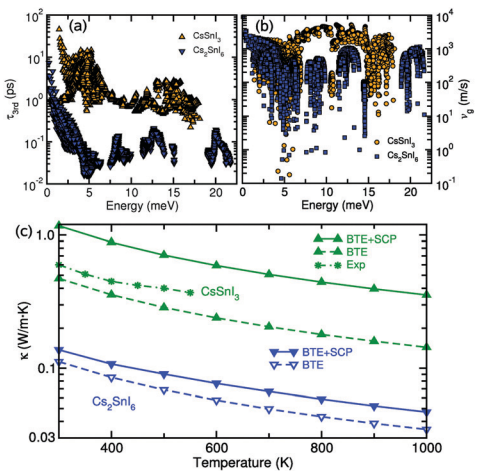

Fig. 2 (a) Phonon lifetimes τ_{3rd}, (b) phonon group velocities v_g, calculated by the self-consistent phonon (SCP) method at 500 K, and (c) temperature-dependent lattice thermal conductivities κ calculated by solving the Boltzmann transport equation (BTE) with harmonic phonons and SCPs, compared with available experimental data[22] for $CsSnI_3$ and Cs_2SnI_6.

Having the necessary quantities of τ, v_g and C_V, we assessed their thermal conductivities as functions of temperature (Fig. 2(c)). When using the SCP energies for solving BTE (BTE + SCP), κ became larger than that calculated using harmonic phonon energies (BTE), as has been found in the previous studies.[25,38,39] For the case of $CsSnI_3$, the calculated values of κ with BTE and BTE + SCP are slightly smaller and larger than the experimental values,[22] indicating a reasonable accuracy of our calculations. As expected from the smaller values of τ, v_g and C_V, the lattice thermal conductivity κ of Cs_2SnI_6 is about a sixth lower than that of $CsSnI_3$ in the temperature range of interest. At 300 K, κ of Cs_2SnI_6 is ultralow at 0.11 W m^{-1} K^{-1} with BTE + SCP, which is a third that of the double perovskite $Cs_2AgBiBr_6$.[25] This ultralow thermal conductivity in an ordered high-symmetry cubic structure Cs_2SnI_6 is unusual with the twofold rattling vibrations as the underlying mechanism.

In summary, we have investigated lattice vibrations and thermal conduction in vacancy-ordered double perovskite Cs_2SnI_6, while comparing with single perovskite $CsSnI_3$. By scrutinizing the crystalline structures and analyzing phonon dispersions and electron localization functions, we conceived that both Cs atoms and isolated SnI_6 octahedra in Cs_2SnI_6 act as twofold rattlers, unlike $CsSnI_3$ with only a Cs atom rattler. We performed anharmonic lattice dynamics calculations, demonstrating that the twofold rattling modes stimulate the lattice anharmonicity and strongly scatter heat-carrying acoustic phonons, thereby resulting in much shorter phonon lifetimes, and slower phonon group velocity in Cs_2SnI_6. We finally calculated the lattice thermal conductivities of Cs_2SnI_6 and $CsSnI_3$ with gradually increasing temperature, revealing the ultralow thermal conductivity of 0.11 W m^{-1} K^{-1} at 300 K in Cs_2SnI_6 with a simple cubic structure.

Un-Gi Jong developed the original project, performed the calculations and drafted the first manuscript. Yun-Sim Kim, Chol-Hyok Ri, Yun-Hyok Kye and Chol-Jin Pak assisted with the DFT calculations and the post-processing of the calculation results, and contributed to useful discussions. Stefaan Cottenier and Chol-Jun Yu supervised the work. All authors reviewed the manuscript.

This work is supported as part of the research project ''Design of New Energy Materials'' (No. 2021-12) by the State Commission of Science and Technology, DPR Korea. Computations were performed on the HP Blade System C7000 (HP BL460c) that is owned by the Faculty of Materials Science, Kim Il Sung University.

Conflicts of interest

The authors declare no competing financial interest.

References

1 L. E. Bell, *Science*, 2008, **321**, 1457–1461.
2 J. Callaway, *Phys. Rev.*, 1959, **113**, 1046–1051.
3 M. G. Holland, *Phys. Rev.*, 1963, **132**, 2461–2471.
4 T. Nishimura, H. Sakai, H. Mori, K. Akiba, H. Usui, M. Ochi, K. Kuroki, A. Miyake, M. Tokunaga, Y. Uwatoko, K. Katayama, H. Murakawa and N. Hanasaki, *Phys. Rev. Lett.*, 2019, **122**, 226601.
5 U. Aseginolaza, R. Bianco, L. Monacelli, L. Paulatto, M. Calandra, F. Mauri, A. Bergara and I. Errea, *Phys. Rev. Lett.*, 2019, **122**, 075901.
6 L. D. Zhao, S. H. Lo, Y. Zhang, H. Sun, G. Tan, C. Uher, C. Wolverton, V. P. Dravid and M. G. Kanatzidis, *Nature*, 2014, **508**, 373–377.
7 Y. Xia, *Appl. Phys. Lett.*, 2018, **113**, 073901.
8 Y. Xia, J. M. Hodges, M. G. Kanatzidis and M. K. Y. Chan, *Appl. Phys. Lett.*, 2018, **112**, 181906.
9 J. Qi, B. Dong, Z. Zhang, Z. Zhang, Y. Chen, Q. Zhang, S. Danilkin, X. Chen, J. He, L. Fu, X. Jiang, G. Chai, S. Hiroi, K. Ohara, Z. Zhang, W. Ren, T. Yang, J. Zhou, S. Osami, J. He, D. Yu, B. Li and Z. Zhang, *Nat. Commun.*, 2020, **11**, 5197.
10 T. Tadano and S. Tsuneyuki, *Phys. Rev. Lett.*, 2018, **120**, 105901.
11 W. Lee, H. Li, A. B. Wong, D. Zhang, M. Lai, Y. Yu, Q. Kong, E. Lin, J. J. Urban, J. C. Grossman and P. Yang, *Proc. Natl. Acad. Sci. U. S. A.*, 2017, **114**, 8693–8697.
12 T. Tadano, Y. Gohda and S. Tsuneyuki, *Phys. Rev. Lett.*, 2015, **114**, 095501.
13 W. Schweika, R. P. Hermann, M. Prager, J. Persson and V. Keppens, *Phys. Rev. Lett.*, 2007, **99**, 125501.
14 M. Christensen, A. B. Abrahamsen, N. B. Christensen, F. Juranyi, N. H. Andersen, K. Lefmann, J. Andreasson, C. R. Bahl and B. B. Iversen, *Nat. Mater.*, 2008, **7**, 811–815.
15 O. Yaffe, Y. Guo, L. Z. Tan, D. A. Egger, T. Hull, C. C. Stoumpos, F. Zheng, T. F. Heinz, L. Kronik, M. G. Kanatzidis, J. S. Owen, A. M. Rappe, M. A. Pimenta and L. E. Brus, *Phys. Rev. Lett.*, 2017, **118**, 136001.
16 D. Zhao, J. M. Skelton, H. Hu, C. La-o-vorakiat, J.-X. Zhu, R. A. Marcus, M.-E. Michel-Beyerle, Y. M. Lam, A. Walsh and E. E. M. Chia, *Appl. Phys. Lett.*, 2017, **111**, 201903.
17 R. X. Yang, J. M. Skelton, E. L. da Silva, J. M. Frost and A. Walsh, *J. Phys. Chem. Lett.*, 2017, **8**, 4720–4726.
18 L. D. Whalley, J. M. Skelton, J. M. Frost and A. Walsh, *Phys. Rev. B*, 2016, **94**, 220301(R).
19 T. Hata, G. Giorgi and K. Yamashita, *Nano Lett.*, 2016, **16**, 2749–2753.
20 S.-Y. Yue, X. Zhang, G. Qin and J. Y. M. Hu, *Phys. Rev. B*, 2016, **94**, 115427.
21 X. Qian, X. Gu and R. Yang, *Appl. Phys. Lett.*, 2016, **108**, 063902.
22 H. Xie, S. Hao, J. Bao, T. J. Slade, G. J. Snyder, C. Wolverton and M. G. Kanatzidis, *J. Am. Chem. Soc.*, 2020, **142**, 9553–9563.
23 S. P. Girdzis, Y. Lin, L. Leppert, A. H. Slavney, S. Park, K. W. Chapman, H. I. Karunadasa and W. L. Mao, *J. Phys. Chem. Lett.*, 2021, **12**, 532.
24 A. D. Wright, L. R. V. Buizza, K. J. Savill, G. Longo, H. J. Snaith, M. B. Johnston and L. M. Herz, *J. Phys. Chem. Lett.*, 2021, **12**, 3352.
25 J. Klarbring, O. Hellman, I. A. Abrikosov and S. I. Simak, *Phys. Rev. Lett.*, 2020, **125**, 045701.
26 U.-G. Jong, C.-J. Yu and Y.-H. Kye, *RSC Adv.*, 2020, **10**, 201.
27 U.-G. Jong, C.-J. Yu, Y.-H. Kye, S.-H. Choe, J.-S. Kim and Y.-G. Choe, *Phys. Rev. B*, 2019, **99**, 184105.
28 A. E. Maughan, A. M. Ganose, A. M. Candia, J. T. Granger, D. O. Scanlon and J. R. Neilson, *Chem. Mater.*, 2018, **30**, 472–483.
29 Y. Cai, W. Xie, H. D. Y. Chen, K. Thirumal, L. H. Wong, N. Mathews, S. G. Mhaisalkar, M. Sherburne and M. Asta, *Chem. Mater.*, 2017, **29**, 7740–7749.
30 C. E. Patrick, K. W. Jacobsen and K. S. Thygesen, *Phys. Rev. B: Condens. Matter Mater. Phys.*, 2015, **92**, 201205.
31 A. E. Maughan, A. M. Ganose, M. M. Bordelon, E. M. Miller, D. O. Scanlon and J. R. Neilson, *J. Am. Chem. Soc.*, 2016, **138**, 8453–8464.
32 A. E. Maughan, A. M. Ganose, M. A. Almaker, D. O. Scanlon and J. R. Neilson, *Chem. Mater.*, 2018, **30**, 3909–3919.
33 Y. Xia and M. K. Y. Chan, *Appl. Phys. Lett.*, 2018, **113**, 193902.
34 U.-G. Jong, Y.-S. Kim, C.-H. Ri, Y.-H. Kye and C.-J. Yu, *J. Phys. Chem. C*, 2021, **125**, 6013–6019.
35 M. K. Jana, K. P. A. Warankar, P. Mandal, U. V. Waghmare and K. Biswas, *J. Am. Chem. Soc.*, 2017, **139**, 4350–4353.
36 A. D. Becke and K. E. Edgecombe, *J. Chem. Phys.*, 1990, **92**, 5397–5403.
37 D. H. Fabini, G. Laurita, J. S. Bechtel, C. C. Stoumpos, H. A. Evans, A. G. Kontos, Y. S. Raptis, P. Falaras, A. Van der Ven, M. S. Kanatzidis and R. Seshadri, *J. Am. Chem. Soc.*, 2016, **138**, 11820–11832.
38 Y. Oba, T. Tadano, R. Akashi and S. Tsuneyuki, *Phys. Rev. Mater.*, 2019, **3**, 033601.
39 T. Tadano and S. Tsuneyuki, *Phys. Rev. B: Condens. Matter Mater. Phys.*, 2015, **92**, 054301.

